Boffin Access

Open Access Journal | Volume: 1.2

Journal of Water Technology and Treatment Methods

Buckminsterfullerene (C60) Nanoparticle Removal by Media Filtration: Is It Unique From Comparable Nanoparticles?

Jonathan A. Brant[1*]
Qiuhong Jia[1]

[1]Department of Civil and Architectural Engineering, University Avenue, Laramie, United States

Abstract

The environmental implications and applications of engineered nanomaterials (ENMs), like buckminsterfullerene (C_{60}), have received considerable interest from stakeholders. Much of this interest is attributed to the belief that ENMs will demonstrate unique behaviors in environmental media, with particular concern paid to nanoparticle mobility (exposure) in aqueous systems. The objective of this study was to compare and contrast the mobility of C_{60} ENMs to that of three differently sized nanospheres having well-defined surface chemistries. The inherent goal was to evaluate the ability of media filtration to remove nanomaterials from aqueous streams. Like the nanospheres, C_{60} mobility was a complex function of size and solution chemistry, and the latter's impact on particle interfacial behavior. Under favorable deposition/attachment conditions C_{60} and nanosphere retention increased with particle size. Nanoparticle mobility in saturated porous media generally followed expectations based on colloid filtration theory until a particle size of approximately 20 nm was reached. Nanoparticles smaller than this critical size demonstrated unique mobility behaviors, which were attributed to the so called nano-effect.

Keywords

Media Filtration; Nanoparticle; Buckminsterfullerene; Transport; Aggregation

Introduction

Sand remains as an important, and often used, media in filtration systems in potable and wastewater treatment systems. It therefore serves as a barrier to a wide-range of contaminants, including Engineered Nanomaterials (ENMs). ENMs like buckminsterfullerene (C_{60}) have elucidated great interest from a variety of manufacturing and scientific fields. As the number of ENM containing commercial products increases so too has interest in understanding their environmental and public health implications [1-13]. An area that has received considerable interest is improving our understanding of ENM mobility across engineered filtration systems [14,15]. Unlike nano-scale metal oxides, like titanium dioxide, C_{60}ENMsdo not have natural colloidal analogs. Coupling this with findings on the possible toxicity of these nanoparticles provides strong motivation for improving our understanding of C_{60} removal in water treatment processes, like media filtration [16].

From the literature, it has been concluded that the following variables affect C_{60} mobility in saturated porous media: the preparation method used to produce the aqueous C_{60}suspension, physical and chemical characteristics of the interacting surfaces, and hydrodynamic conditions within the porous media [17-25]. Chen and Elimelech found that the method used to produce aqueous suspensions of C_{60} clusters (nC_{60}) affected their mobility in the porous media [21]. This was due to difference in the physical and chemical properties of the nanoparticles, which differ according to preparation method used [26]. Lecoanet and Wiesner also studied the mobility of different types of nC_{60} and determined that derivitized forms were more mobile relative to non-derivitized ones [27]. This was explained in terms of differences in attachment efficiencies to the collector media, which were lower for the derivitized forms of the nC_{60}. The importance of the attachment efficiency in determining ENM removal was highlighted by Hassan et al., [28]. These researchers determined that slow sand filters serve as poor barriers to cerium dioxide ENMs irrespective of their influent concentration under constant particle loading conditions [28]. This was attributed to the low attachment efficiency between the cerium dioxide and the sand media. According to Espinasse et al, solution ionic strength, Darcy velocity, and the presence of organic matter all affected the mobility of nano-C_{60}in porous media [19]. The influences of organic matter on nC_{60} mobility and their aggregation state have been studied in detail by different research groups [19,29-31]. These efforts collectively found that like for colloids, organic matter is capable of adsorbing to C_{60} surfaces resulting in enhanced electrostatic and steric interactions, and in turn greater mobility in aqueous systems. A general conclusion from these earlier efforts is that in many ways, C_{60} mobility in saturated porous media is similar to that of colloidal materials and is generally affected by the same variables. In other words,

Article Information

DOI: 10.31021/jwt.20181110
Article Type: Research Article
Journal Type: Open Access
Volume: 1 **Issue:** 2
Manuscript ID: JWT-1-110
Publisher: Boffin Access Limited

Received Date: March 21, 2018
Accepted Date: March 29, 2018
Published Date: March 31, 2018

*Corresponding author:

Jonathan A. Brant
Department of Civil and Architectural Engineering
University of Wyoming
1000 E. University Avenue, Laramie
United States
Tel: (307) 766 – 5446
Fax: (307) 766 – 2221
E-mail: jbrant1@uwyo.edu

Citation: Jonathan BA, Jia Q. Buckminsterfullerene (C60) Nanoparticle Removal By Media Filtration: Is It Unique From Comparable Nanoparticles? J Water Technol Treat Methods. 2018 Mar;1(2):110

C_{60} removal by sand media is expected to be a function of the two efficiency terms that contribute to filtration efficiency: attachment efficiency and collision efficiency.

The objective of this study was to determine if C_{60} displays unique mobility characteristics in saturated porous media, representative of filter media, relative to other nanoparticles having similar surface chemistries. Specific goals associated with meeting the overall objective this research effort included: (i) evaluate the role of Derjaguin-Landau-Verwey-Overbeek (DLVO) interactions in determining C_{60} mobility in saturated porous media, (ii) characterize the relationship between mobility and particle size, and (iii) establish whether surrogate nanoparticles may be used for predicting the mobility and removal of C_{60} in and by porous media.

Theoretical

Clean-bed filtration theory has been found to adequately describe the mobility of nano-scale clusters of C_{60} (nC_{60}) in saturated porous media [19,23,26,32]. In clean-bed filtration theory, particle mobility is a product of the collision efficiency (η_0) and attachment efficiency (α) between a given particle and collector surface. The attachment efficiency, α is the fraction of particle collisions, either with each other or with the collector surface, that result in particle attachment [33]. Both physical and chemical interactions can contribute to α. The significance of these interactions (physical and chemical) is a function of particle size and in turn the nanoparticle aggregation state [34]. The attachment efficiencyα between particle and collector surfaces was determined from packed column experiments using Equation 1:

$$a = -\frac{4r_c}{3(1-\varepsilon)\eta_0 L} 1n(\frac{C}{C_0}) \quad (1)$$

Where r_c is the collector radius; L is the length or depth of the porous media bed; η_0 is the single collector collision efficiency, which for nanoparticles is primarily due to diffusion; C and C_0 are respectively the effluent and influent (L = 0) nanoparticle concentrations to the packed column [35]. Another approach for calculating α involves batch adsorption tests to characterize nanoparticle adsorption onto collector surfaces. Adsorption capacity (A) is defined as the mass of nanoparticles (M_n) that contact and adsorb to some unit mass of collectors (M_c) at a given condition.

$$A = \frac{M_n}{M_c} \quad (2)$$

The A is normalized to the maximum observed adsorption capacity (A_{max}) to determine α.

$$\alpha = \frac{A}{A_{\max}} \quad (3)$$

Where A_{max} is the adsorption rate under favorable attachment conditions. Theoretically, α is a function of the surface energy components of any two interacting surfaces. Nanoparticle attachment to the filter media was assessed within the context of the extended Derjaguin–Landau–Verwey–Overbeek (XDLVO) model [36]. In the XDLVO model the total interaction energy between two surfaces is the summation of electrostatic (E_{EDL}), VanderWaals (E_{LW}), and acid-base(E_{AB}) interactions. To model these interactions one must determine the surface energy components of the relevant surfaces. The EL component is modeled using zeta potential as a surrogate parameter for surface charge. The LW and AB surface energy components must be calculated based on measured contact angles formed between the relevant solid surface and a polar and polar liquid.

The Surface Element Integration (SEI) technique (Equation 4) was used to scale each of the interaction energy components as a function of separation distance assuming a sphere-plategeometry [37]. The SEI technique computes the total interaction energy between two bodies by numerically integrating the interaction energy per unit area between two differential elements over the entire surface. This approach uses a cylindrical coordinate system with the origin located at the center of the particle. Each interaction energy component (E) is function of separation distance (h), which his integrated over the entire particle radius (a).

$$E_{SEI} = 2\pi \int_0^a \left[E\left(D + a - a\sqrt{1-\left(\frac{r}{a}\right)^2} \right) - E\left(D + a - a\sqrt{1-\left(\frac{r}{a}\right)^2} \right) rdr \right] \quad (4)$$

Where D is the separation distance between the two interacting surfaces (sphere-plate);and r is the radial coordinate in the polar coordinate system.

The hydraulic conditions within the filter media were characterized in terms of the Reynolds and Peclet numbers. The Reynolds number was calculated according to Equation 5.

$$R_e = \frac{\rho_w \nu d}{\mu} \quad (5)$$

Where Re is the Reynolds number for flow around a spherical collector; ρ_w is the density of water at the relevant temperature; v is the filtration rate (superficial velocity); d is the collector diameter; and μ is the dynamic viscosity of water at the relevant temperature. The Peclet number, *Pe,* which describes the relative significance of advection and dispersion in particle transport to a collector surface, was determined using Equation 6.

$$P_e = \frac{3\pi\mu d_p d\nu}{K_B T} \quad (6)$$

Where d_p is the particle diameter; k_B is the Boltzmann constant; and T is the absolute temperature.

Experimental

a. Reagents

All salts used in this study were acquired from Fisher Scientific and were reagent grade or better. Ultrapure water, having a resistivity of 18 mΩ-cm and an average pH = 7.5, was used to make all test solutions. Solution ionic strength was adjusted using reagent grade sodium chloride. (Fisher Scientific).

b. Characterization of nanoparticle and filter media surface chemistry

Nanoparticle and collector surface chemistry was characterized with respect to their van der Waals (γ^{LW}), electron acceptor (γ^+), and electron donor (γ^-) surface energy components. These components were determined using the procedure detailed in Brant and Childress [36]. Contact angles were measured using the sessile drop technique on thin-films of the respective nanoparticles. Nanoparticles were deposited onto a non-porous membrane (TFC-XR, Koch Membranes Systems) to form a thin-film. For these tests, 300 mL of a 5 mg L^{-1} particle suspension was permeated through the membrane using a dead end filtration apparatus. As the water permeated through the membrane the nanoparticles were rejected to form a thin-film on top of the membrane. When permeation was complete the membrane was removed and dried for a minimum of 24 hrs in a dessicator cabinet. The dried membrane was then cut into strips and placed into a holder to prevent curling. The membrane was then placed on the goniometer stage and the contact angle was measured using the sessile drop method. Contact angles were measured using a computer interfaced goniometer (Easy Drop, Kruss Scientific, Hamburg, Germany). All measurements were done with a liquid droplet volume of 5 µL. Measurements were done using two polar (ultrapure water and formamide) probe liquids and a single a polar (diiodomethane) probe liquid. The surface energy components of these liquids that were used in this work have been reported elsewhere [36]. Average contact angles were calculated based on a minimum of five contact angles measured per sample on no less than three different samples.

c. Surface Charge

Particle surface charge (zeta potential) was calculated from measured electrophoretic mobility values. Electrophoretic mobility was measured using laser Doppler velocimetry and phase analysis light scattering. Zeta potential was calculated from electrophoretic mobility using the Smoluchowski approximation which is valid for systems where the thickness of the electric double layer is much less than the particle radius [38]. Electrophoretic mobility was measured as a function of solution ionic strength and pH through automatic titration using concentrated solutions of sodium chloride, sodium hydroxide, and/or hydrochloric acid. Zeta potential as a function of solution ionic strength was measured by adjusting the solution pH to 7.0 and then titrating the sample with a 1 M sodium chloride solution. Streaming potential measurements (Surpass Electrokinetic Analyzer) were done on the glass spheres to calculate a zeta potential using the Helmholtz-Smoluchowski equation [38]. Streaming potential was measured at two different solution ionic strengths (2 and 10 mM potassium chloride) as a function of solution pH, which was adjusted using potassium hydroxide and hydrochloric acid.

d. Nanoparticle Size and Aggregation State

Nanoparticle size was measured using a combination of dynamic light scattering (DLS, Zetasizer, Malvern Instruments) and Transmission Electron Microscopy (TEM, Hitachi H-7000). DLS was used to measure the mean hydrodynamic diameter (d_h), number weighted size distribution, and intensity weighted size distributions of the nanoparticle suspensions. TEM measurements were done by placing a dilute droplet of a nanoparticle suspension onto a copper mesh grid that was air dried for 10 mins. Nanoparticle size, and its evolution (aggregation), were measured as a function of solution pH and ionic strength.

e. Nanoparticles

Crystalline buckminsterfullerene (C_{60}) [purity = 99.95%] was purchased from the Materials and Electrochemical Research Corporation and used without further purification. Suspensions of stable C_{60} aggregates (nC_{60}) were synthesized using the methodology previously detailed by Andrievsky et al., [39]. ThenC_{60}suspensions were passed through a hydrophilic 0.45 µm filter to remove any large aggregates prior to their use. The filtrate was stored in a sealed brown glass container at 5°C. Multiple batches of nC_{60} were prepared and used to form a single stock solution having a concentration of 16 mg L^{-1}. Based on TEM images of the nC_{60} the nanoparticles had a spherical geometry with diameters ranging from 20 to 60 nm (Figure 1).

Spherical nanospheres, composed of a polystyrene core and a hydroxylated surface coating, were obtained from Phosphorex Inc. Nanospheres having diameters of 25 nm, 50 nm and 100 nm were used. Nanospheres were used to develop comparative mobility assessments for ENMs having the same surface chemistry, but different, yet narrow, size distributions. The hydroxylated surface of the nanospheres, approximates that of the nC_{60}. It has previously been determined that the nC_{60} can be approximated as a hydrophobic core having hydroxyl surface groups [27]. In this way the nanospheres were used as surrogates for the nC_{60} where the particle size would be carefully controlled for drawing a comparative analysis to the nC_{60}.

f. Filter Media

Borosilicate glass spheres (Potters Industries Inc.) were used as filter media in this study. The size of the glass spheres were determined using sieve analysis with 425 µm and 150 µm sized meshes and using Field Emission Electron Microscopy (FESEM). Those fractions of media that were smaller than the 425 µm mesh, but retained by the 150 µm mesh sieve were used in filtration studies. These fractions of media were further characterized using FESEM. The size distribution of the glass spheres was determined through analysis of FESEM images of the media. The glass spheres had a relatively narrow size distribution (150 to 425 µm), a mean diameter of 308 µm, and were spherical in geometry (Figure 2). The measured isoelectric point (pH_{iep}) for the glass spheres was2.2. The contact angle with water for glass was 21.7° ± 3.0, with corresponding calculated surface energy values of γ^{LW} = 36.5, mJ m^{-2}, γ^{+}= 1.9 mJ $m^{-2}$and γ^{-}= 48.3 mJ m^{-2}.

g. Batch adsorption tests

Batch adsorption tests were done under varying pH and ionic strength conditions to quantify the affinity of the nC_{60} and nanospheres to the different filter media. For the batch adsorption tests as a function of solution pH, a series of three 30mL nC_{60} aqueous suspensions having an ionic strength of 10 mM NaCl and nC_{60} = 5 mgL^{-1}were prepared in 50 mL Teflon bottles. Solution pH was adjusted to values of 3, 7, or10 using hydrochloric acid or sodium hydroxide. Initial and subsequent nanoparticle concentrations were measured using UV-Vis analysis. The mass of glass spheres (= 15 g per vessel) used in the adsorption tests was based on a surface area ratio of the media to nC_{60} of 64:1. The nC_{60}-media mixture was mixed for 48 hrs using a rotary mixer, after which the media was allowed to settle out of suspension. A similar procedure was followed when investigating the effect of ionic strength (0, 1, 10, or 100 mM, pH = 7) of adsorption.

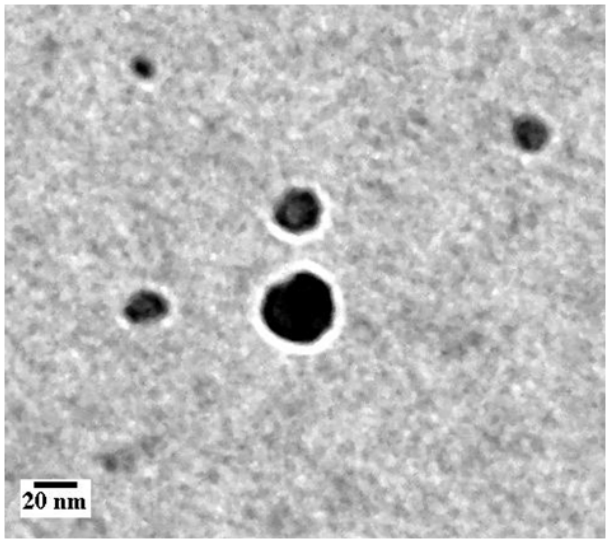

Figure 1: Representative TEM image of nC_{60} in ultrapure water. The mean nanoparticle size for the reported TEM image was 21.9 ± 9.2 nm (n = 27).

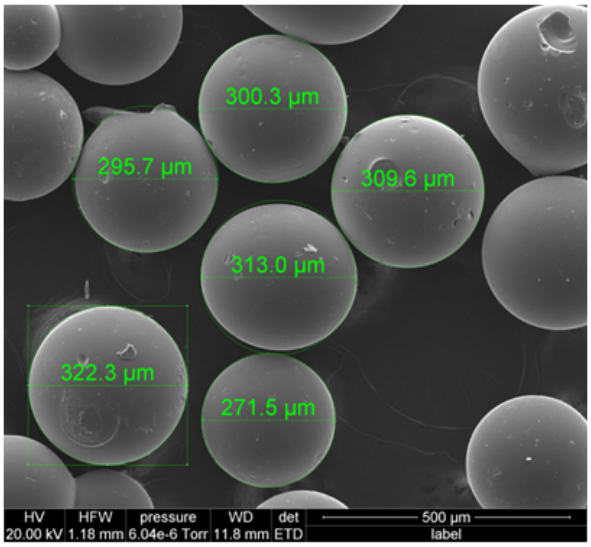

Figure 2: Representative FESEM image of the glass spheres used in the nanoparticle filtration experiments.

h. Media filtration test apparatus

All filtration experiments were done using a packed column apparatus consisting of a syringe pump (Model 33, Harvard Apparatus), column (C Column, GE Health Care), and a flow-through UV-Vis system (UV-1800, Shimadzu). The UV-Vis system included a flow-through quartz cell for measuring the effluent particle concentration from the column as a function of time. The column had an inner diameter of 16 mm and a length of 20 cm. The media bed height for all tests was 18 cm accounting for the retaining mesh used to prevent displacement of the media during the filtration tests. The porosity and pore volume of the packed column were determined using gravimetric analysis, where the pore volume was equal to the mass of water retained by the media bed. The average porosity and pore volume of the glass spheres were 0.43 ± 0.02 and 16.3 mL, respectively. The measured porosity for the glass media approximated that of sand (0.4 to 0.43) used in potable rapid rate filtration systems.

i. Nanoparticle filtration experimental procedure

All filter media was cleaned prior to use. The media was soaked in a 1 M hydrochloric acid solution for 12 hours and then rinsed with ultrapure water. It was then placed in a beaker and sequentially sonicated for 30 min in solutions of 0.01 M sodium hydroxide, ultrapure water, 1 M nitric acid, and then ultrapure water. The media was dried in an oven set at 110ºC for 24 hrs and then loaded into the column. As the media was loaded into the column it was agitated to remove voids and facilitate consolidation. When the packed column was placed into the test apparatus it was flushed with a minimum of 10 pore volumes of ultrapure water to further consolidate the media. A tracer test was done prior to each mobility test using nitric acid to assess the media's hydraulic characteristics. After each tracer test, the column was flushed with a minimum of 10 pore volumes of ultrapure water and then 10 pore volumes of the background electrolyte solution that was used in the subsequent filtration experiment. The background electrolyte solution was allowed to equilibrate with the media for at least 30 mins prior to flushing. All solutions were pumped through the packed column in an up-flow configuration.

Nanoparticle suspensions (C_o = 5 mg/L) were prepared using a 1 M sodium chloride solution to adjust ionic strength, followed by pH adjustment using hydrochloric acid or sodium hydroxide. Prior to each test, the nanoparticle suspension was mixed on a roller mixer for 1 hr to ensure that it had reached an equilibrium aggregation state, at which point its size and zeta potential was measured. After the tracer test was completed and the column was flushed with 10 pore volumes of the background electrolyte solution, the nanoparticle suspension was injected into the bottom of the column. Once at least 10 pore volumes of the nanoparticle suspension had passed through the column the feed was switched to the background electrolyte solution to observe the descending portion of the breakthrough curve. All experiments were done at a superficial velocity of 0.07 cm/sec (2.52 m/hr), which corresponded to pore velocities (v_{pore}) of 0.16 cm/sec for the glass spheres. The superficial velocity used here are on the lower end of the spectrum for rapid rate media filters, which employ velocities of 5 to 15 m/hr, but higher than those used in slow sand filtration (0.08 to 0.25 m/hr). The hydraulic conditions for those tests using the glass media were laminar based on the calculated Reynolds number (Re= 0.21). Because Re < 1 the flow through the media was characterized as creeping flow (viscous flow behavior), where the fluid followed distinct streamlines through the media. For all experimental combinations $Pe \sim 10^4$, indicating that advection was the primary transport mechanism.

Results and Discussion

Contact angle with water and surface energy values (γ^{LW}, γ^+, γ^-) for the nC_{60} and hydroxylated nanospheres are reported in Table 1. Both types of nanoparticles were hydrophobic based on their contact angles with water (~90°). The cores of both nanoparticles are hydrophobic moieties, carbon in the case of the nC_{60} and polystyrene for the nanospheres. Similarly, both had hydroxyl surface groups, which impart a negative surface charge over a pH range of 3 to 10 (Figure S2). The negative surface charge of the nC_{60} is in agreement with previous studies [18]. The nC_{60} were more negatively charged than the nanospheres over the studied ionic strength (Figure S3) and pH conditions. The largest nanosphere (d_p = 100 nm) was characterized by a more negative zeta potential under any given condition relative to that measured for the 25 nm and 50 nm nanospheres; however, the magnitudes of the zeta potential values for each of the nanospheres were comparable.

a. Nanoparticle Behavior in Water

The intensity and number weighted d_h values for the nanoparticles are reported as a function of solution chemistry in Table 2. At pH 7 the critical coagulation concentration for the nC_{60} was 100 mM. At this point, the height of the energy barrier (φ_{max}) between two interacting nC_{60} was 0 kT, compared to 225 kT at 10 mM (pH 7). At 10 mM the nC_{60} were stable over a pH range of 3 to 10, though some increase in particle size was observed at pH 3. Similar results were obtained for the three different nanosphere size fractions. Exceptions to this observation were that each of the nanosphere size fractions aggregated at pH 3 (10 mM) and that the 100 nm sized nanospheres remained stable at 100 mM (pH 7). Based on these results all of the nanoparticles were charge stabilized; however, the magnitude of the interfacial interactions scaled with particle size.

b. Filtration of Nc_{60} by Model Media

From Figure 3, retention of the $nC_{60}$was minimal at ≤ 10 mM; however, it increased to an average value of 74%at 100 mM. The breakthrough profiles shown in Figure 3 followed expectations based on DLVO theory. The φ_{max} decreased from 260 kT to 0 kT for the nC_{60}-glass system as the ionic strength increase from 10 to 100 mM at pH 7.The higher retention at 100 mM may be attributed, at least in part, to nC_{60} aggregation and the affinity of free flowing nC_{60} for previously deposited nanoparticles resulting in an increase in α (Table 2). If the interfacial interaction between any two nanoparticles is repulsive, as was the condition at ≤ 10 mM, then they should elute from the column once the available attachment sites in the glass media are exhausted. Physical straining/blocking may also have played a role particularly at 100 mM and would have occurred at the contact points between the glass spheres. The average pore size in the glass media (d_{pore}= 46.4 µm) was at least three orders of magnitude larger than the aggregated nanoparticles resulting in a d_p/d_{pore} = 0.01. Physical straining was expected to become a primary removal mechanism at a $d_p/d_{pore} \geq 0.05$[41]; however it could occur if the interstitial pore size has become reduced through particle attachment.

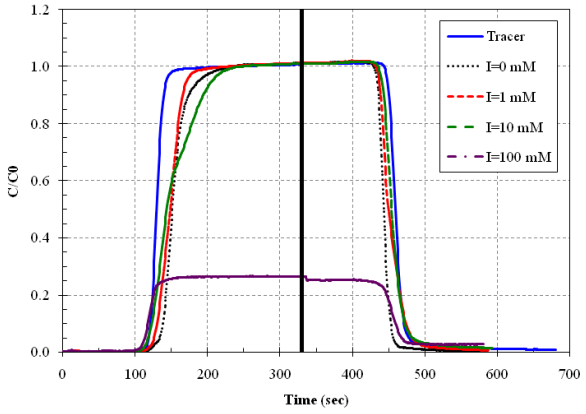

Figure 3: Average breakthrough curves forthe nC_{60}through the glass packing media as a function of solution ionic strength (ε = 0.454; T=23°C; v_{Darcy} = 0.07 cm sec^{-1}; v_{Pore} = 0.154 cm sec^{-1}; n = ≥ 2, pH 7 ± 0.05). The feed was switched to the particle free background electrolyte solution at t = 330 secs (black vertical line).

	nC_{60}	Nanospheres		
		25 nm	50 nm	100 nm
Zeta Potential (10 mM))				
pH = 3	-20.5	-13.8	-7.9	-7.9
pH = 7	-48.5	-11.0	-11.0	-27.4
pH = 10	-61.8	-23.2	-27.0	-31.0
Zeta Potential (pH = 7)				
I = 1 mMNaCl	-54.3	-31.8	-29.3	-37.5
I = 10 mMNaCl	-48.5	-11.8	-12.0	-27.4
I = 100 mMNaCl	-27.9	-3.0	-3.0	-10.1
θ_{water}	95.0°± 2.8°	87.8° ± 9.4°		
Surface Energy				
$\gamma^{LW}(mJ/m^2)$	43.16	41.45		
$\gamma^{+}(mJ/m^2)$	0.61	6.84		
$\gamma^{-}(mJ/m^2)$	1.66	17.18		

Table 1: Zeta potential, contact angle with water and corresponding surface energy values for the nC_{60} and hydroxylated Polystyrene nanospheres.

	Hydrodynamic Diameter, nm (pH7)				Hydrodynamic Diameter, nm (10 mM)	
	0 mM	1 mM	10 mM	100 mM	pH3	pH10
nC_{60}	110.5 (41.1)	138.1 (47.4)	112.4 (38.5)	542.0 (43.0)	151.5 (69.0)	117.9 (37.0)
25 nm	35.3 (23.4)	34.2 (20.8)	31.3 (24.3)	146.2 (26.0)	126.6 (28.9)	30.5 (22.0)
50 nm	60.2 (46.5)	57.8 (45.1)	60.1 (43.5)	90.3 (48.2)	81.1 (45.5)	62.1 (43.7)
100 nm	98.8 (81.8)	95.0 (77).0	95.1 (78.3)	98.0 (81.8)	143.8 (80.9)	98.0 (85.2)

Table 2: Intensity (number) weighted hydrodynamic diameters for the nanoparticles under those solution chemistries used in the mobility experiments ($n \geq 3$, T=25°C).

The attachment efficiencies for the nC_{60} to the glass media based on the breakthrough curves ($\alpha_{Breakthrough}$), were relatively low for ≤ 10 mM (pH 7), which was due to the poor nanoparticle retention that was measured under these conditions. At 100 mM the $\alpha_{Break\ through}$ was 22% (retention= 74%) compared to 0.1% at 10 mM. A more dramatic contrast was observed in the α values calculated from the batch adsorption experiments (α_{Batch}). The α_{Batch} increased from approximately 6.4% at 1 mM to 74% at 100 mM. The calculated φ_{max} between the nanoparticles and glass media under the aforementioned conditions decreased from approximately 260 kT to 0 kT. The higher α that was determined through the batch measurements, relative to that determined using clean bed filtration theory, may be attributed to a variety of factors, such as the differences in the mixing, or contacting, conditions in the two types of experiments [33].

From Figure 4, nC_{60} elution was highest ($C/C_o \sim 1.0$) and retention lowest at pH ≥ 7, and was more rapid at pH 10. At pH 3, nC_{60} retention in the glass media was nearly complete (= 97%) further indicating that nC_{60} attachment was charge regulated. The high retention at pH 3 can be attributed to the aggregated state of the nC_{60} under these conditions, resulting in pore blockage over time and the high affinity of nanoparticles in the bulk solution to nanoparticle deposits on the glass media. These scenarios may be evidenced by the increase in nanoparticle retention over time seen in Figure 4 at pH 3. Another consideration is the relatively low energy barrier (φ_{max}= 11 kT) between the nanoparticles and glass media. While the overall retention values were similar at pH ≥ 7 there were distinct differences in the shapes of the respective breakthrough profiles. At pH 10 the break through time for the nC_{60} was comparable to that for the tracer indicating negligible retention within the media (Figure 4). At pH 7 the inflection point in the breakthrough profile points to some retention within the media, and the retention increasing after roughly 140 secs. The increase in retention may be attributed to the creation of favorable attachment sites in the form of nanoparticle deposits on the glass media. It is also possible that the nanoparticles are accessing different flow paths as the test proceeds. This could happen as the most accessible flow paths become blocked by deposited particles in the beginning of the test resulting in the nanoparticles being forced to take longer, more tortuous flow paths.

The α_{Batch} values for the nC_{60} and glass at pH 7 (0.14 ± 0.03) and pH 10 (0.24 ± 0.06) were higher relative to $\alpha_{Breakthrough}$, with the exception to those values determined at pH 3.At pH 3, $_{Breakthrough}$ (0.85 0.03) and α_{Batch} (0.71 ± 0.18) were comparatively similar, which agreed with the high retention values (~ 97%) that were measured. The α_{Batch} results suggest that nanoparticle attachment to the glass media can, and does, occur at both pH 7 and 10; however, retention within the glass media under these conditions was negligible. Note that there was no statistical difference in the α_{Batch} values determined at pH 7 and 10 (P = 0.087,> 0.05). It is interesting that such a low average retention value was obtained at pH 10 despite a relatively high α_{Batch} value. Thus, v_{pore} may be of sufficient magnitude relative to the adhesive force between the nanoparticle(s) and glass to prevent fixed attachment.

c. Predictors of nanoparticle retention

The same mobility experiments that were done for the nC_{60} were carried out using the three different nanosphere size fractions to identify what variable may best be used to predict nanoparticle

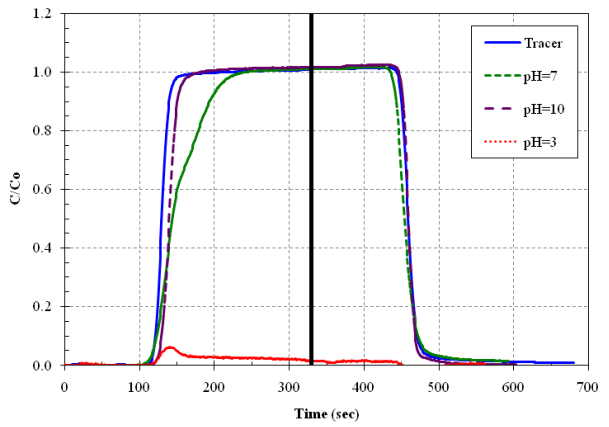

Figure 4: Average breakthrough curves forthe nC_{60}through the glass packing media as a function of solution pH (I = 10 mMNaCl; ε = 0.454; T=23°C; v_{Darcy} = 0.07 cm sec^{-1}; v_{Pore} = 0.154 cm sec^{-1}; n ≥ 2). The feed was switched to the particle free background electrolyte solution at t = 330 secs (black vertical line).

mobility. Two different conditions were considered: 1) unfavorable attachment (pH 7, pH 10 at 1 mM and 10 mM, respectively) and 2) favorable attachment (pH 3, 10 mM and pH 7, 10 and 100 mM). Representative breakthrough profiles for the unfavorable attachment conditions for then$C_{60}$and three different nanosphere size fractions are summarized in (Figure 5). All of the different nanoparticles were highly mobile, with minimal retention in the glass media. The 50 nm nanospheres exhibited a marginally higher retention (= 3.2%) relative to the other nanoparticles. Under these conditions each of the nanoparticles was stable suggesting weak interactions with particle deposits if present. The *α Breakthrough* values for the nanoparticles were approximately zero. At pH 7 the interaction energy profiles for the nanoparticles and glass media were characterized by a repulsive energy barrier, with φ_{max} increasing for the nanospheres from 12 to 116 kT as d_h increased from 34 to 95 nm. The nC_{60}were similarly sized as the 100 nm nanospheres; however, their number weighted d_h (47.4 nm) was more comparable to the 50 nm nanospheres (45.1 nm) (Table 2). Under the unfavorable attachment all of the nanoparticles had similar breakthrough profiles (Figure 5a).

Distinctly different breakthrough profiles were observed for the three nanosphere size fractions when the solution pH and ionic strength were increased to 10 and 10 mM, respectively relative to that seen at 1 mM (pH 7). From each of the nanospheres exhibited non-monotonic break through profiles (Figure 5b). The non-monotonic breakthrough may be attributed to a variety of factors like interactions with previously deposited particles and/or the blocking of favorable flow paths by particles deposits (short-circuiting). Therefore, it was difficult to assign a specific retention values under these conditions. Even when the feed flow was switched to the nanoparticle-free background electrolyte solution, the C/C_o value continued to increase with time, suggesting that particles were being released from the glass media. The relative breakthrough order for the nanospheres under these conditions was that the 100 nm nanospheres were most mobile while the 50 nm nanospheres were least mobile. In comparison, the nC_{60} were not retained to an appreciable extent in the glass media under these conditions. No obvious trends between nanoparticle retention and energy barrier height or particle size, existed to explain the observed results.

Breakthrough curves for then C_{60} and the three different nanosphere size fractions under the favorable deposition conditions are summarized in Figure 6**.** The nC_{60} were poorly retained (0.6%) by the glass media under these conditions; however, the nanospheres were each retained to varying degrees unlike what was observed at 1 mM and pH 7 (Figure 6a) (Figure 5a). The 25 nm nanospheres were the least retained (4.7%), while both the 50 nm and 100 nm nanospheres were better retained by the glass media. The C/C_o plateau values for both the 50 nm and 100 nm nanospheres did not reach a steady-state value and instead tended to creep upward with time similar to what was observed at pH 10 (Figure 5b). Interestingly the 100 nm nanospheres were less mobile in the glass media under these conditions relative to the 25 nm nanospheres as opposed to what was seen at pH 10. The error associated with interpreting these non-monotonic profiles hinders making definitive conclusions about the differences in nanosphere mobility. Increasing the solution ionic strength to 100 mM (pH 7), or reducing the solution pH to 3 (10 mM), resulted in the relative disappearance of the non-monotonic breakthrough profiles for the nanospheres (Figure 6b-6c). Additionally, the retention of the nanospheres by the glass media under these conditions now followed more convention as retention increased with increasing particle size based on the number weighted d_h (Table 2). If particle size is interpreted in terms of the intensity weighted d_h then size no longer correlates with retention. The disappearance of the non-monotonic breakthrough behavior for the nanospheres suggests that its origins lay in the interfacial interactions between the nanospheres themselves in solution and with the glass media; however, it is not captured in the interfacial and transport

To better understand what role, if any, particle size and interfacial conditions played in determining particle mobility the average retention values for the different nanoparticles were plotted as a function of number weighted d_h and φ_{max}. Recall that some breakthrough profiles for the nanospheres were non-monotonic in nature and thus determining an exact value for R was difficult. Also,

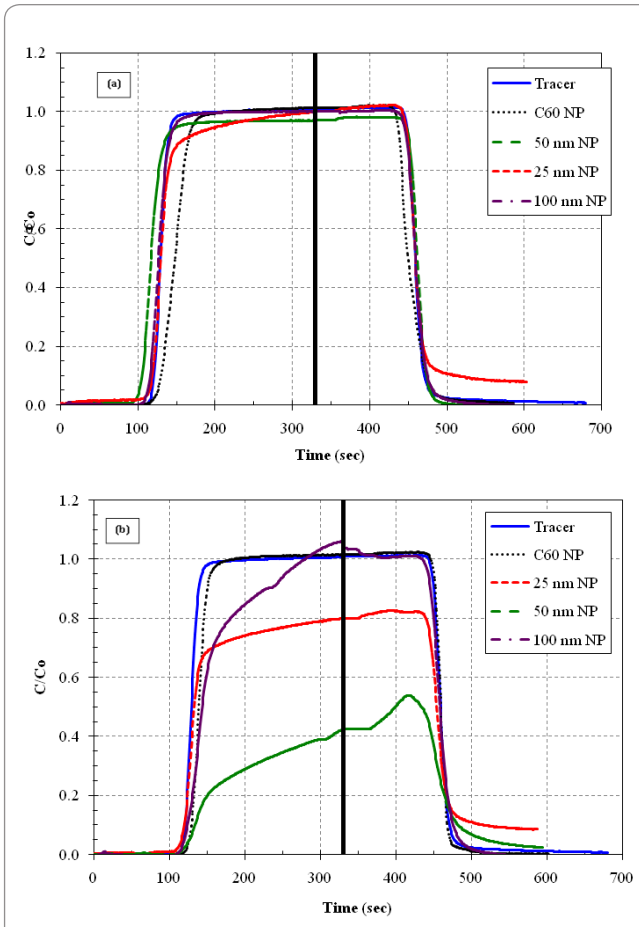

Figure 5: Average breakthrough curves for the nC_{60} and three nanosphere size fractions under unfavorable attachment conditions in the saturated glass media. Condition 1 was (a) 1 mM NaCl and pH 7, while Condition 2 was (b) 10 mM NaCl and pH 10 ε = 0.454; T=23°C; v_{Darcy} = 0.07 cm sec^{-1}; v_{Pore} = 0.154 cm sec^{-1}; n ≥ 2).

the reported d_h for any nanoparticle is the that which existed for the particle solution entering into the packed column. From Figure 7a, there appears to be a reasonably good correlation between retention and particle size. This relationship best describes those conditions characterized as favorable for attachment. When attachment conditions were less favorable the correlation becomes less strong or disappears all together. One consideration is that under unfavorable attachment conditions retention is expected to be zero and thus no correlation with particle size would be expected. At least for favorable attachment conditions and/or when particle aggregation had occurred particle mobility was inversely proportional to particle size.

Plotting the average retention value for each of the different nanoparticles as a function of φ_{max} found no correlation between these two variables (Figure 7b). No correlation existed for the global population of nanoparticles regardless of whether the intensity or number weighted d_h (the number weighted value is reported in Figure 7b was used to calculate the φ_{max}. There are however, a number of interesting observations that may be made from Figure 7b. First, is the linear (R^2 = 0.9) relationship between retention and φ_{max} that existed for the 25 nm nanospheres. Mobility increased (decreasing retention) for the 25 nm nanosphere as φ_{max} decreased, which is counter to conventional expectations where we would expect mobility to decrease as the interfacial conditions become more favorable for attachment. The observations made here cannot be attributed to differences in nanosphere size, which would affect the calculated $_{max}$, as the number weighted d_h remained between 20 to 29 nm for all of the tested solution chemistries. The opposite scenario existed for the nC_{60} where mobility increased (minimal to no retention) onceφ_{max} was ≥ 20 kT. The number weighted d_h for the nC_{60} was comparable to the 50 nm nanosphere under all of the tested conditions though their retention values were distinctly different (Table 2). This may be attributed to at least two different factors: 1) the comparatively higher polydispersity of the nC_{60} suspension makes it more difficult to describe the system with a single calculate a single φ_{max} value, and 2) the nature of the breakthrough profiles for the nanospheres makes determining a single retention value complex at best.

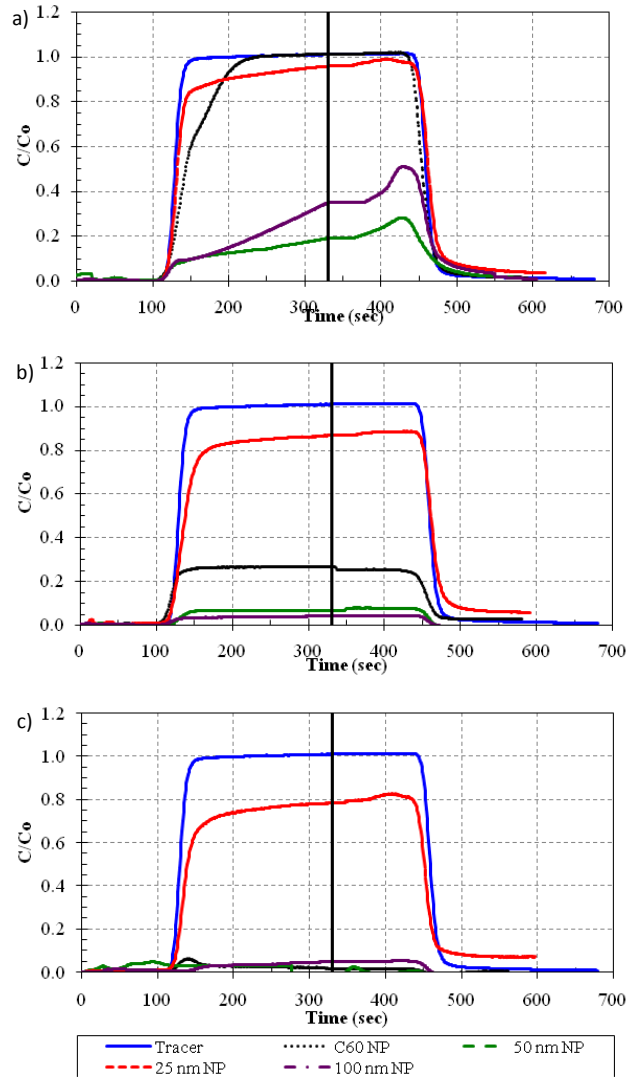

Figure 6: Average breakthrough curves for the nC_{60} and three nanosphere size fractions under favorable attachment conditions in the saturated glass media. Condition 1 was (a) I = 10 mM NaCl and pH 7; Condition 2 was (b) I = 100 mM NaCl and pH 7, and condition 3 was (c) I = 10 mM NaCl and pH 3 (ε = 0.454; T=23°C; v_{Darcy} = 0.07 cm sec^{-1}; v_{Pore} = 0.154 cm sec^{-1}; n ≥ 2).

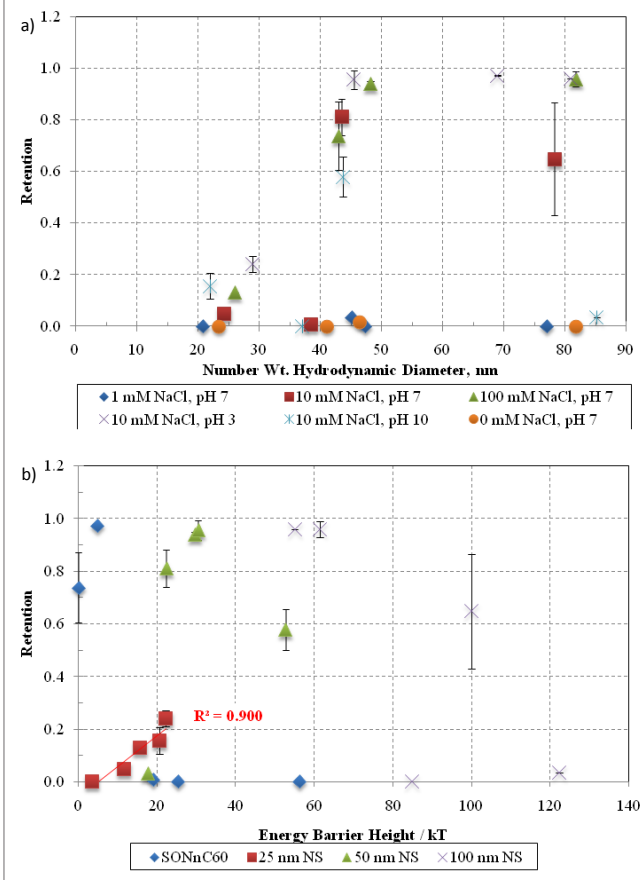

Figure 7: Nanoparticle retention as a function of (a) mean number weighted hydrodynamic diameter (d_h) and (b) interfacial interaction energy barrier height (φ_{max}).

Conclusions

ENMs, like C_{60}, are often associated with, or predicted to have, unique behaviors in engineered and natural environments. Based on the results presented here, C_{60} nanoparticles, or aggregates, do not possess mobility characteristics in saturated porous media, representative of that used in conventional filtration processes, which are unique from that displayed by other nano-scale particles having similar size and surface chemistries. Instead, like other materials their mobility is a function of both size and surface chemistry. The XDLVO model, combined with the SEI scaling technique, provided a reasonably good prediction for when a nanoparticle transitions from being mobile in saturated porous media to immobile. Under favorable deposition/attachment conditions nanoparticle retention by the media increased with particle size. Nanoparticle mobility followed conventional expectations until a size of approximately 20 nm was

reached. At and below this size the nanoparticles demonstrated unique mobility behaviors, which may be attributed to the so called nano-effect.

Acknowledgements

The authors gratefully acknowledge Dr. Tzahi Cath from the Colorado School of Mines for his assistance with the streaming potential measurements for the glass spheres.

References

1. Foundation N. S., National Nanotechnology Initiative National Nanotechnology Initiative Overview. 2006.
2. Adams LK, Lyon DY, Alvarez PJJ. Comparative eco-toxicity of nanoscale TiO2, SiO2, and ZnO water suspensions. Water Research. 2006 Nov;40(19):3527-3532
3. Lyon DY, Adams LK, Falkner JC, Alvarez PJJ. Antibacterial activity of fullerene water suspensions: effects of preparation method and particle size. Environ. Sci Technol. 2006 Apr;40:4360-4366
4. Fortner JD, Lyon DY, Sayes CM, Boyd AM, Falkner JC, et al. C60 in water: nanocrystal formation and microbial response. Environ Sci Technol. 2005;39 Apr:4307-4316
5. Li Q, MahendraShaily, Lyon Delina Y, Brunet Lena, Li Dong, et al. Antimicrobial nanomaterials for water disinfection and microbial control: Potential applications and implications. Water Research. 2008 Nov;42(18):4591-4602
6. Lyon DY, Alvarez PJJ. Fullerene Water Suspension (nC60) Exerts Antibacterial Effects via ROS-Independent Protein Oxidation. Environmental Science and Technology. 2008 Oct;42(21):8127-8132
7. Lyon DY, Fortner JD, Sayes CM, Colvin VL, Hughes JB. Bacterial cell association and antimicrobial activity of a C60 water suspension. Environmental Toxicology and Chemistry. 2005 Feb;24:2757-2762
8. Oberdörster E, Zhu S, Blickley TM, McClellan-Green P, Haasch ML. Ecotoxicology of carbon-based engineered nanoparticles: Effects of fullerene (C60) on aquatic organisms. Carbon. 2006 May;44(6):1112-1120
9. Ringwood AH, Levi-Polyachenko N, Carroll DL. Fullerene Exposures with Oysters: Embryonic, Adult, and Cellular Responses. Environ Sci Technol. 2009 Sep;43:7136-7141.
10. SayesCM, Gobin AM, Ausman KD, Mendez J, West JL, et al. Nano-C60 cytoxicity is due to lipid peroxidation. Biomaterials. 2005 Dec;26:7587-7595.
11. Yu-Nam Y, Lead J R. Manufactured nanoparticles: an overview of their chemistry, interactions and potential environmental implications. Sci Total Environ. 2008 Aug,400(1-3):396-414.
12. Brant JA, Koyuncu I, Lecoanet H, Veerapaneni S, Wiesner MR. Characteristics and Occurrence of Nano-Scale Particles in Filter Process Streams. Journal of American Water Works Association. 2011;103(12):46-60.
13. Lee H, Segets D, Sub S, Peukert W, Pui DYH. Liquid filtration of nanoparticles through track-etched membrane filters under unfavorable and different ionic strength conditions: Experiments and modeling. J Memb Sci. 2017 Feb;524:682-690.
14. Matsuda S, Matsui S, Shimizu Y, Matsuda T. Genotoxicity of Colloidal Fullerene C60. Environ SciTechnol 2011 Apr;45(9):4133–4138.
15. Elimelech M, Chen LK. Relating Colloidal Stability of Fullerene (C60) Nanoparticles to Nanoparticle Charge and Electrokinetic Properties. Environ Sci Technol. 2009 Apr;43(19):7270-7276.
16. Brant JA, Lecoanet HF, Hotze M, Wiesner MR. Comparison of electrokinetic properties of colloidal fullerenes (n-C60) formed using two procedures. Environ Sci Technol. 2005 Sep;39:6343-6351.
17. Espinasse B, Hotze EM, Wiesner MR. Transport and Retention of Colloidal Aggregates of C60 in Porous Media: Effects of Organic Macromolecules, Ionic Composition, and Preparation Method. Environ Sci Technol. 2007 Oct;41(21):7396-7402.
18. Brant JA, Lecoanet H F, Wiesner MR. Aggregation and deposition characteristics of fullerene nanoparticles in aqueous systems. J Nanopart Res. 2005 Oct;7:545-553.
19. Chen KL, Elimelech M. Relating colloidal stability of fullerene (C60) nanoparticles to nanoparticle charge and electrokinetic properties. Environ Sci Technol. 2009 Oct;43:7270-7276.
20. Jiemvarangkul P, Zhang Wx, Lien HL. Enhanced transport of polyelectrolyte stabilized nanoscale zero-valent iron (nZVI) in porous media. Chem Eng J. 2011 Jun;170(2-3):482-491.
21. Lecoanet HF, Bottero JY, Wiesner MR. Laboratory Assessment of the Mobility of Nanomaterials in Porous Media. Environ Sci Technol. 2004 Aug;38(19):5164-5169.
22. Zhang WX. Nanoscale iron particles for environmental remediation: An overview. J Nanopart Res. 2003 Aug;5(3-4):323-332.
23. Chen KL, Elimelech M. Aggregation and deposition kinetics of fullerene (C60) nanoparticles. Langmuir. 2006 Nov;22(26):10994-11001.
24. Lecoanet H, Wiesner MR. Velocity Effects on Fullerene and Oxide Nanoparticle Deposition in Porous Media. Environ. Sci. Technol. 2004;38(16):4377-4382.
25. Brant JA, Labille J, Bottero JY, Wiesner MR. Characterizing the Impact of Preparation Method on Fullerene Cluster Structure and Chemistry. Langmuir. 2006 Mar;22(8):3878-3885.
26. Isaacson CW, Bouchard DC. Effects of humic acid and sunlight on the generation and aggregation state of aqu/nC60 nanoparticles. Environ Sci Technol. 2010 Nov;44(23):8971-8976.
27. Hassan AA, Li Z, Sahle-Demessie E, Sorial GA. Computational fluid dynamics simulation of transport and retention of nanoparticle in saturated sand filter. J Hazard Mater. 2013 Jan;244-245:251-258.
28. Li Q, Xie B, Hwang YS, Xu Y. Kinetics of fullerene dispersion in water enhanced by natural organic matter and sunlight. Environ. Sci. Technol. 2009 Apr;43(10):3574-3579.
29. Xie B, Xu Z, Guo W, Li Q, Impact of natural organic matter on the physicochemical properties of aqueous C60 nanoparticles. Environmental Science and Technology. 2008;42(8):2853-2859.
30. Jaisi DP, Saleh NB, Blake RE, Elimelech M. Transport of Single-Walled Carbon Nanotubes in Porous Media: Filtration Mechanisms and Reversibility. Environmental Science and Technology 2008;42:8317-8323.
31. Solovitch N, Labille J, Rose J, Chaurand P, Borschneck D, et al. Concurrent Aggregation and Deposition of TiO2 Nanoparticles in a Sandy Porous Media. Environmental Science and Technology. 2010;44(13):4897-4902.
32. Schrijver JHM, Vreeken C, Wesselingh JA. Deposition of particles on a cylindrical collector. Journal of Colloid and Interface Science. 1981;81(1):249-256.
33. Kim DS, Hong SB, Kim YJ, Lee KW. Deposition and coagulation of polydisperse nanoparticles by Brownian motion and turbulence. Journal of Aerosol Science. 2006;37(12):1781-1787.
34. Brant JA, Childress AE. Assessing short-range membrane-colloid interactions using surface energetics. Journal of Membrane Science. 2002;203:257-273.
35. Hoek, EMV, Agarwal GK. Extended DLVO interactions between spherical particles and rough surfaces. J Colloid Interface Sci. 2006 Jun 1;298(1):50-58.
36. M. Elimelech JG, X Jia RA, Williams. Particle Deposition and Aggregation: measurement, modelling and simulation. Butterworth-Heinemann 1995.
37. Andrievsky GV, Kosevich MV, Vovk OM, Shelkovsky VS, Vanshchenko LA. On the production of an aqueous colloidal solution of fullerenes. Journal of the Chemical Society. Chemical Communications. 1995;(12):1281-1282.
38. Crittenden JC, Trussell RR, Hand DW, Howe KJ, Tchobanoglous G. Water Treatment Principles and Design. Third Edition ed.; John Wiley & Sons, Inc.: Hoboken, New Jersey. 2012;1901.
39. Sakthivadivel R. Theory and mechanism of filtration of non-colloidal fines through a porous medium; University of Berkeley: 1966;220.